RSC Advances

PAPER

View Article Online
View Journal | View Issue

Cite this: *RSC Adv.*, 2019, **9**, 19333

Fe_3O_4/SO_3H@zeolite-Y as a novel multi-functional and magnetic nanocatalyst for clean and soft synthesis of imidazole and perimidine derivatives

Mehdi Kalhor * and Zohre Zarnegar

Received 17th April 2019
Accepted 3rd June 2019

DOI: 10.1039/c9ra02910a

rsc.li/rsc-advances

In this study, SO_3H@zeolite-Y was synthesized by the reaction of chlorosulfonic acid with zeolite-NaY under solvent-free conditions, which was then supported by Fe_3O_4 nanoparticles to give SO_3H@zeolite-Y (Fe_3O_4/SO_3H@zeolite-Y) magnetic nanoparticles. Several techniques were used to evaluate the physical and chemical characterizations of the zeolitic nanostructures. Fe_3O_4-loaded sulfonated zeolite was applied as a novel multi-functional zeolite catalyst for the synthesis of imidazole and perimidine derivatives. This efficient methodology has some advantages such as good to excellent yield, high purity of products, reusability of nanocatalyst, simple reaction conditions, environmental friendliness and an economical chemical procedure from the viewpoint of green chemistry.

1. Introduction

Nitrogen-containing heterocyclic compounds including imidazole and perimidine have attracted significant interest over the past decade due to their widespread applications.[1–3] They are predominantly used as antimicrobial, antiulcer, anti-inflammatory, antifungal, antitumor, antibiotic, anti-thrombotic, and therapeutic agents.[4–6] Some of the imidazole and perimidine molecules with biological activities are presented in Fig. 1.[7–9]

Imidazole was first reported in 1858 by Heinrich Debus *via* cyclocondensation of glyoxal, formaldehyde, and ammonia.[10] Various synthetic methods have already reported the synthesis of substituted imidazoles by varying the functional groups on reactants. The tri-substituted imidazoles have been synthesized *via* multicomponent reaction using 1,2-dicarbonyl compounds, different aldehydes, and a nitrogen source in the presence of acidic catalysts.[11–18] Although these reported catalytic methods are very useful and effective in some aspects, they may have some limitations and difficulties such as strongly acidic conditions, occurrence of side reactions, long reaction time, and require harsh reaction conditions, and complex work-up and purification.

Perimidines or 1*H*-benzo[*d*,*e*]quinazolines as saturated N-heterocycles are valuable molecules in the pharmaceutical industry, agriculture, and synthetic chemistry. Perimidine derivatives are usually prepared through condensation reaction of 1,8-diaminonaphthalene with various carbonyl compounds.[19–21] However, most of reported methods suffers from long reaction times, cumbersome work-up procedures, solvents and low yield reactions.[20,21] Thus, the development of suitable and fantastic methods is still desirable for the synthesis of perimidines and highly substituted imidazoles especially by using highly active, robust, stable, and green catalysts.

Recently, magnetic separations have been introduced as optional approach for recovering and reusing catalysts in chemical catalytic procedures. Magnetic nanocatalysts are heterogeneous catalytic systems with advantages of simple recovery and reuse after completion of reactions. Among the various types of magnetic catalysts, the sulfonic acid functionalized heterogeneous catalyst based on the magnetic systems show excellent catalytic activities, high stability, easy preparation and reusability, enhanced selectivity, operational simplicity, and more economically viable processes. In this context, different types of magnetic SO_3H-bearing organic and inorganic compounds used in catalytic reactions such as sulfonic acid magnetic graphene oxide for synthesis of indazolophthalazinetriones,[22] Fe_3O_4@MCM-48–SO_3H for the synthesis of benzo[*f*]chromeno[2,3-*d*]pyrimidinones,[23] Fe_3O_4@-PEG400-SO_3H and its use in Paal–Knorr reaction,[24] Fe_3O_4@-SiO_2–SO_3H for the synthesis of amidoalkyl naphthols,[25] cobalt ferrite chitosan sulfonic acid magnetic nanoparticle for one-pot, four-component synthesis of 2*H*-indazolo[2,1-*b*]phthalazine-triones,[26] SO_3H-functionalized magnetic-titania nanoparticles for the synthesis of benzimidazoquinazolinones and polyhydroquinolines,[27] and *etc.*[28] To the best of our knowledge, there is no report for the application of magnetic SO_3H-functionalized zeolite in chemical organic reactions.

Over the past decade, the use of zeolites as heterogeneous catalysts or ideal supports for homogeneous catalysts have been employed for some catalytic processes due to their attractive properties such as high surface area, nanoporous crystalline

Department of Chemistry, University of Payame Noor, P. O. Box 19395-4697, Tehran, Iran. E-mail: mekalhor@gmail.com; Fax: +98 2537179170; Tel: +98 2537179170

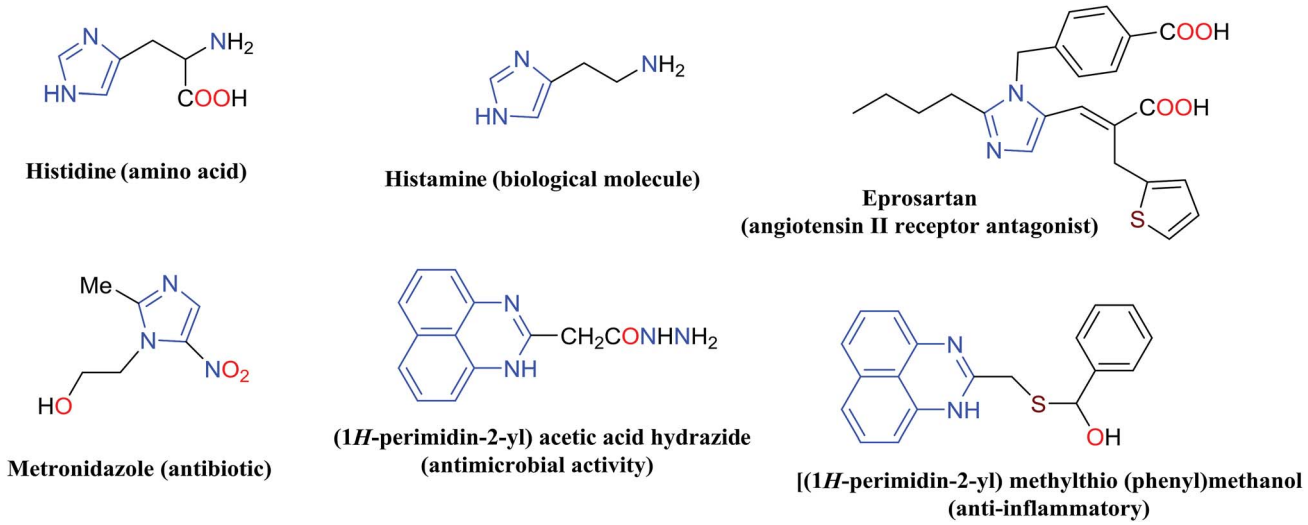

Fig. 1 Some of the imidazoles and perimidines with medicinal properties and biological activities.

structure, less or no corrosion, high thermostability, persistence in all organic solvents, no waste or disposal problems, easy set-up of continuous processes, *etc.*[29,30] Although various SO_3H-activated zeolites used for catalytic reactions,[31] direct methanol fuel cell application,[32] and as temperature tolerant proton conducting material,[33] but there is no example of the use of magnetic SO_3H-modified zeolite-NaY in order to design efficient a heterogeneous catalyst for the synthesis of N-containing heterocycles.

In the present research, an eco-friendly and simple synthetic method have been developed for the preparation of the imidazole and perimidine heterocycles by using of Fe_3O_4 magnetic nanoparticles supported on zeolosulforic acid (Fe_3O_4/SO_3H@zeolite-Y) nanocomposite as a magnetic solid acid catalyst (Scheme 1).

2. Results and discussion

2.1. Characterization of nanocatalyst

As shown in Scheme 2, zeolite-NaY was functionalized with SO_3H groups, which has an affinity with positive ferrous and ferric ions. After the addition of ammonium hydroxide solution, Fe_3O_4 nanoparticles were formed on the surface of SO_3H@zeolite-Y. A systematic study was carried out for the characterization of the synthesized Fe_3O_4/SO_3H@zeolite-Y.

Fig. 2 shows the SEM images of the zeolite-NaY, SO_3H@zeolite-Y and Fe_3O_4/SO_3H@zeolite-Y. In Fig. 2a, it is obvious that the zeolite-NaY has a crystalline structure. As Fig. 2b shows, the structure of SO_3H@zeolite-Y is similar to that of the pristine zeolite with a rougher surface. Moreover, it can be observed from Fig. 2c that the surface of magnetic zeolite is rough after being coated with Fe_3O_4. Fig. 2d clearly shows, the Fe_3O_4 nanoparticles are distributed on the surface of SO_3H@zeolite-Y. The above mention results indicate that zeolite was successfully coated with magnetic particles.

The composition of Fe_3O_4/SO_3H@zeolite-Y was analyzed by energy dispersive X-rays (EDX) and the results are presented in Fig. 3. Elemental analysis results confirm the Fe element in the modified zeolite structure.

The XRD determination was carried out to acquire crystalline structural information on Fe_3O_4/SO_3H@zeolite-Y. The XRD patterns of magnetic zeolite supported SO_3H is shown in Fig. 4. The main peaks at 2θ values of 30.56°, 35.96°, 43.66°, 53.94°, 57.59°, 63.20° and 74.97° are belong to crystal indexes of (220), (331), (400), (422), (511), (440) and (533), respectively. The obtained results are consistent with standard XRD data of Fe_3O_4 (JCPDS no. 01-1111), indicating that Fe_3O_4 has been successfully made. According to Scherrer's equation, the equivalent particle size could be calculated as about 10 nm.

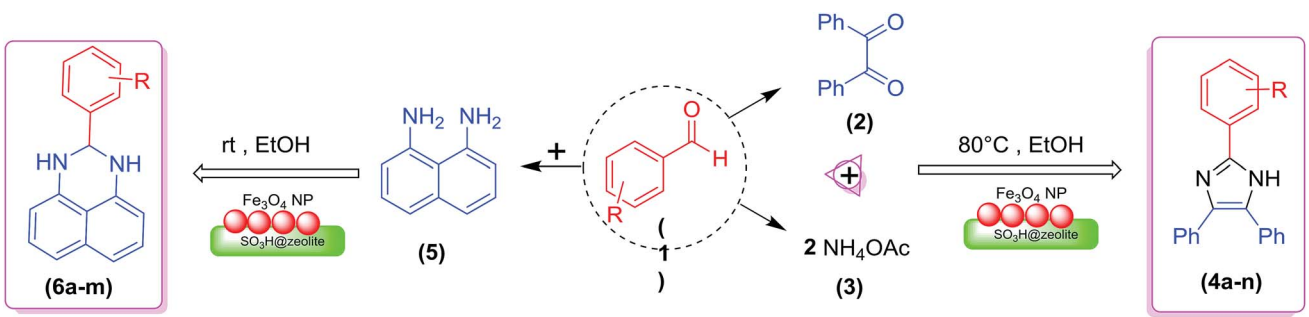

Scheme 1 The synthetic pathway of imidazole and perimidine heterocycles using Fe_3O_4/SO_3H@zeolite-Y.

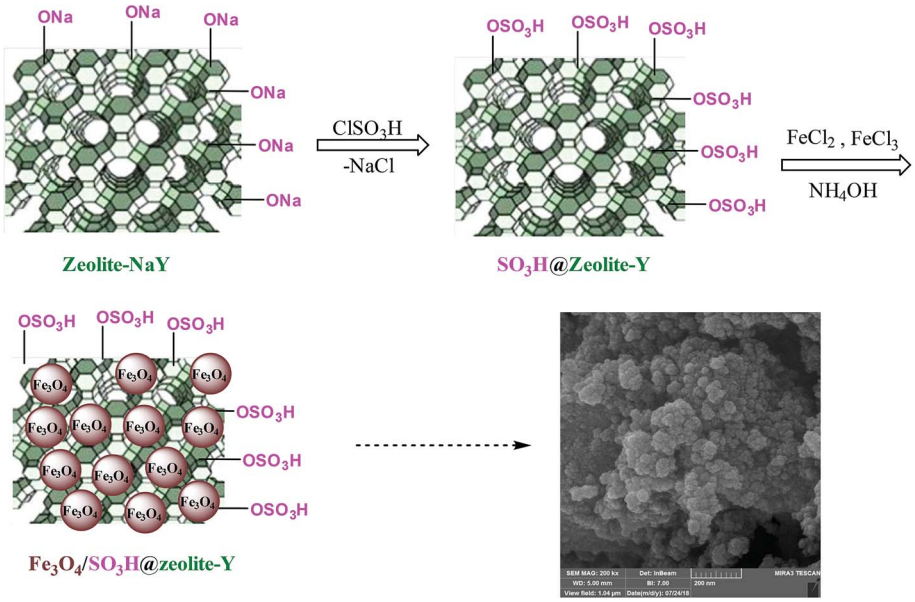

Scheme 2 Simplified schematic representation of the preparation of Fe_3O_4/SO_3H@zeolite-Y.

A comparison is made between, FT-IR spectra of zeolite-NaY, SO_3H@zeolite-Y and Fe_3O_4 zeolitic structures. In the spectrum of zeolite-NaY, in Fig. 5a, the broad absorption band in 3459 cm^{-1} region is related to the O–H stretching of hydrogen bonded internal silanol groups and hydroxyl stretching of water, while the peak at 1636 cm^{-1} corresponds to the O–H

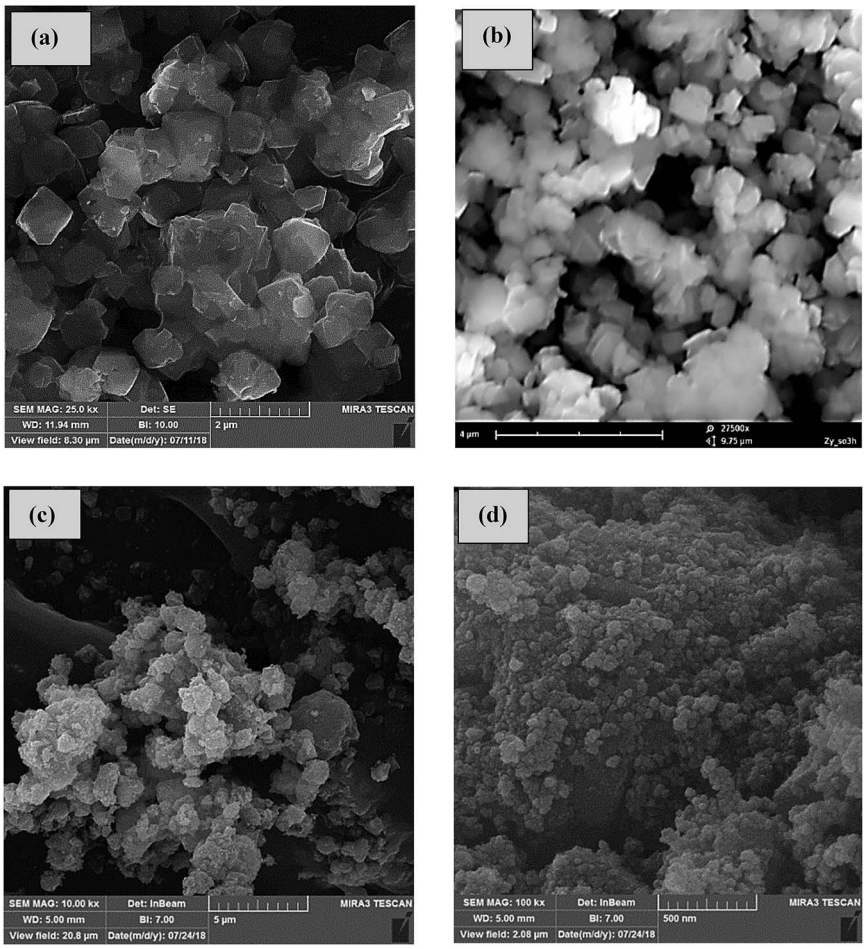

Fig. 2 FESEM photographs of (a) zeolite-NaY, (b) SO_3H@zeolite-Y, (c) and (d) Fe_3O_4/SO_3H@zeolite-Y.

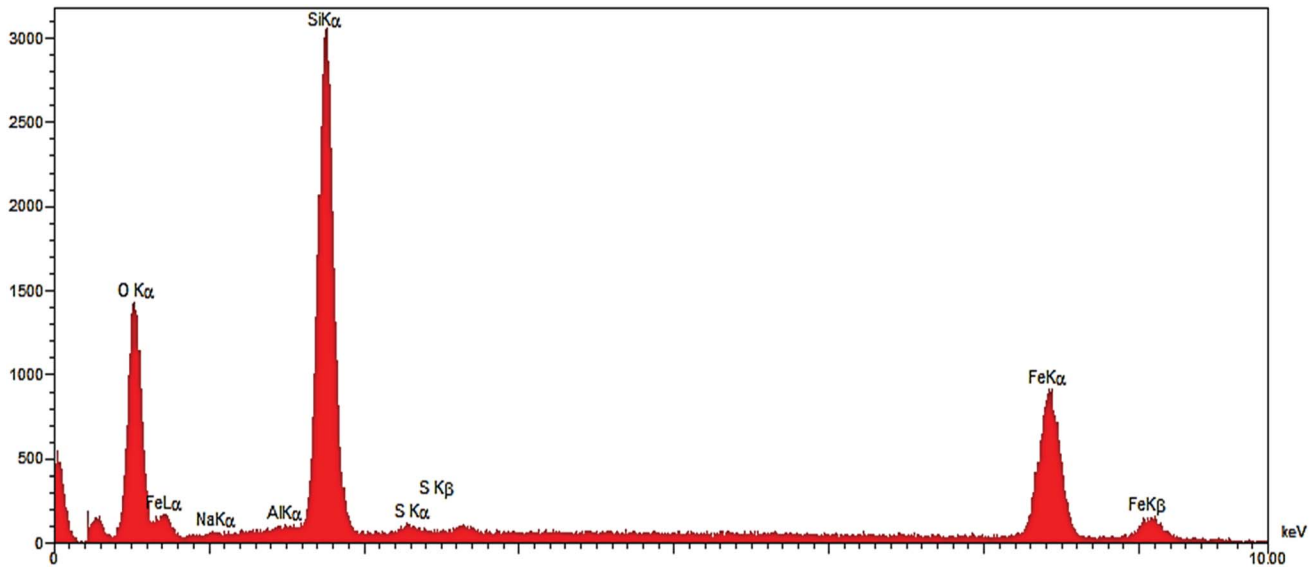

Fig. 3 The EDX spectrum of Fe_3O_4/SO_3H@zeolite-Y.

group bending mode of water. Moreover, the absorption bands 1021 and 792 cm^{-1} are attributed to the symmetric and asymmetric stretching vibrations of the Si–O–Si groups, respectively. In FT-IR spectrum of SO_3H@zeolite (Fig. 5b), the broad band at 3420 cm^{-1} is related to the stretching vibrations of O–H groups. There is an adsorption band at 1635 cm^{-1} for OH bending vibration belonging to physically adsorbed H_2O. The absorption band around 1087 cm^{-1} is related to the Si–O stretching vibration and the asymmetric and symmetric stretching of S=O bond. The bands at 945 and 798 cm^{-1} maybe assigned to the S–O bond. The band at 455 cm^{-1} is attributed to the bending vibrations of Si–O–Si or Al–O–Si groups for the modified zeolite-NaY. FT-IR spectrum of Fe_3O_4/SO_3H@zeolite-Y in Fig. 5c, reveals the presence of all adsorption band corresponding to SO_3H@zeolite. Further, the existence of peak at 576 cm^{-1} corresponds to the stretching vibrations of Fe–O groups indicates that magnetic Fe_3O_4 nanoparticles is supported on sulfonated zeolite.

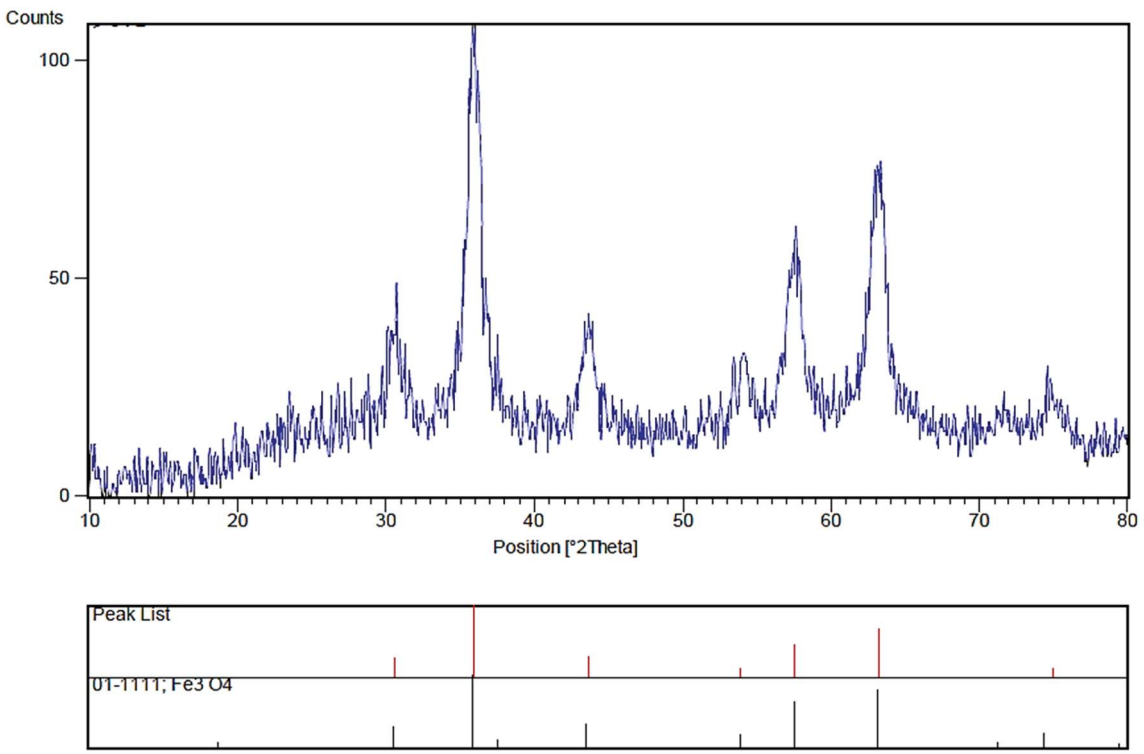

Fig. 4 XRD pattern of Fe_3O_4/SO_3H@zeolite-Y.

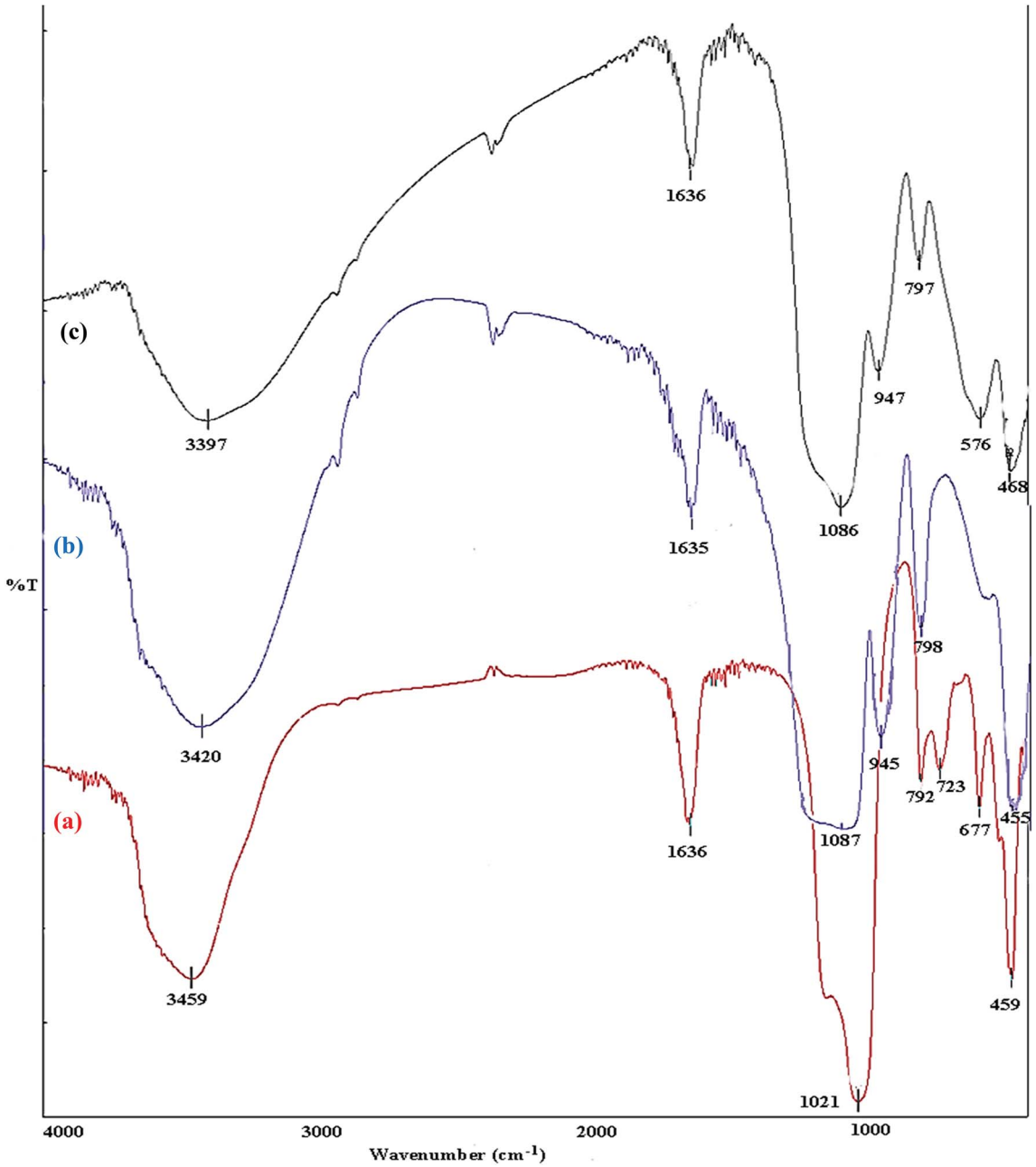

Fig. 5 FTIR spectra of (a) zeolite-NaY, (b) SO_3H@zeolite-Y and (c) Fe_3O_4/SO_3H@zeolite-Y.

Nitrogen adsorption–desorption isotherm analysis and BJH pore size distributions were carried out to evaluate the surface and structure properties of Fe_3O_4/SO_3H@zeolite-Y. As shown in Fig. 6, the N_2 adsorption–desorption isotherm of Fe_3O_4/SO_3-H@zeolite-Y displays an H1-type hysteresis loop and BJH pore distribution curve of type IV which is in agreement with typical mesostructure. Also, by looking at its hysteresis type, it can be seen that Fe_3O_4/SO_3H@zeolite-Y has slits (layer and layer with high pores) structure and the initial nanostructure after the functionalize is still retained,[35] The structure data of all these materials are summarized in Table 1. The BET surface area (205.68 $m^2\ g^{-1}$) and average pore diameter (6.7767 nm) were recorded for Fe_3O_4/SO_3H@zeolite-Y. The BET surface area is decreased relative to SO_3H@zeolite-Y (284.84 nm). These results confirm successful supporting of Fe_3O_4 in the pores of SO_3H functionalized zeolite-NaY.[36] The Fe_3O_4/SO_3H@zeolite-Y has a higher pore volume (6.77 nm) in comparison with sulfonated zeolite-Y (2.35 nm), which might be due to the presence of magnetic nanoparticles through the zeolite cavities.

The magnetization curve of magnetic SO_3H@zeolite nanocomposites is shown in Fig. 7. The saturation magnetization is found to be 21.30 emu g^{-1}. With this saturation magnetization values, it could be rapidly separated from its liquid dispersions under a magnetic field. These results indicate that Fe_3O_4/SO_3-H@zeolite-Y exhibits enough magnetic response to meet the need of magnetic separation.

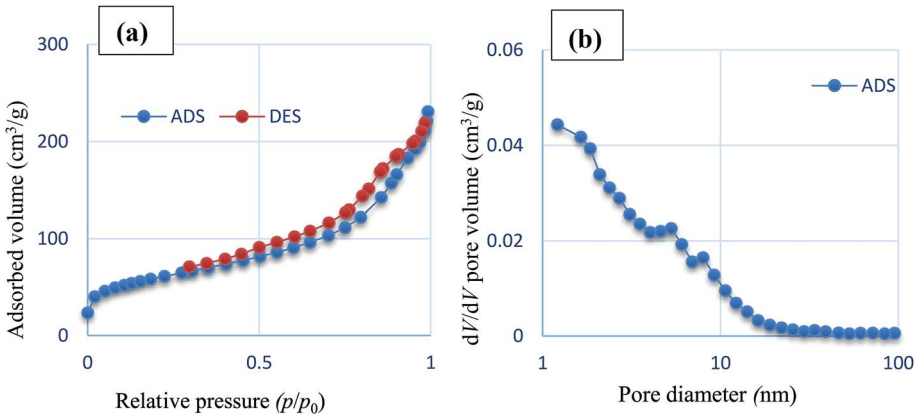

Fig. 6 (a) Nitrogen adsorption–desorption isotherm and (b) BJH pore size distributions of Fe_3O_4/SO_3H@zeolite-Y.

Table 1 Porosimetery values for zeolite-NaY and its modified structures

Samples	S_{BET} [a] ($m^2\ g^{-1}$)	V_{BJH} [b] ($cm^3\ g^{-1}$)	D_{BJH} [c] (nm)	D_{Aap} [d] (nm)
Zeolite-NaY	619.66	0.0667	4.84	2.2358
SO_3H@zeolite-Y	284.84	0.0532	5.15	2.3517
Fe_3O_4/SO_3H@zeolite-Y	205.56	0.0348	2.42	6.7767

[a] Specific surface area. [b] Pore volume. [c] Pore size (calculated from the adsorption branch). [d] Adsorption average pore diameter ($4V/A$) by BET.

2.2. The catalytic activity of Fe_3O_4/SO_3H@zeolite-Y in the synthesis of imidazole and perimidine derivatives

At first, the catalytic ability of Fe_3O_4/SO_3H@zeolite-Y has been investigated for the synthesis of various substituted imidazoles. To optimize the reaction conditions for the synthesis of 2,4,5-triarylsubstituted imidazoles, the reaction of the benzaldehyde (1 mmol), benzil (1 mmol) and ammonium acetate (2 mmol) was considered as a model reaction. To find the optimized nanocatalyst ratio, different amounts of the magnetic zeolite were evaluated in EtOH solvent. The obtained results were listed in Table 2. The best quantity of the Fe_3O_4/SO_3H@zeolite-Y for the preparation of tri-substituted imidazoles was 0.02 g (Table 2, entry 3). By increasing the amount of the nanocatalyst the reaction yield decreased (Table 2, entries 4 and 5). In the next step, the catalytic reaction was carried out in the various solvents like EtOH, MeOH, CH_3CN, H_2O, EtOH : H_2O (1 : 1), DMSO, and CH_2Cl_2 under reflux conditions (Table 2, entries 3 and 6–11). The best yield was obtained in EtOH solvent. The

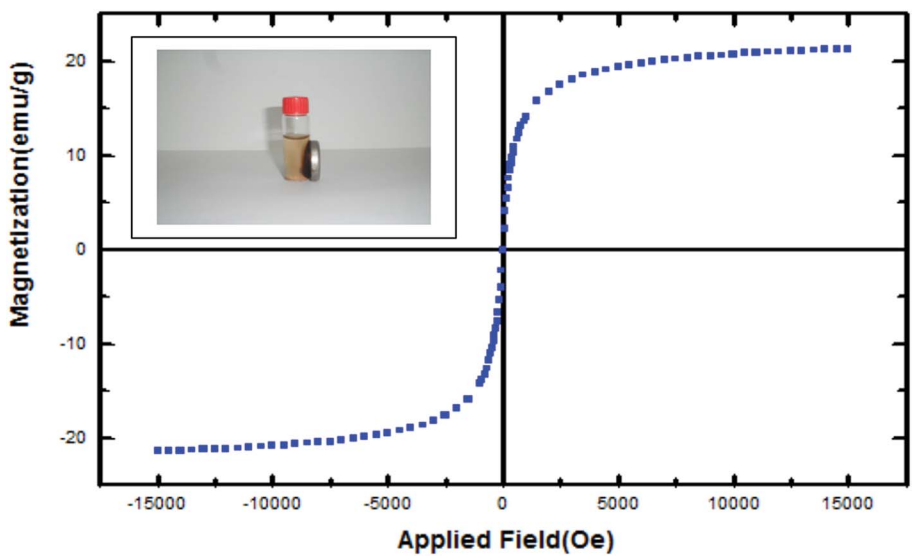

Fig. 7 Field-dependent magnetization curve measured at room temperature for Fe_3O_4/SO_3H@zeolite-Y.

Table 2 Optimizing the model reaction conditions for the synthesis of imidazole **4a**[a]

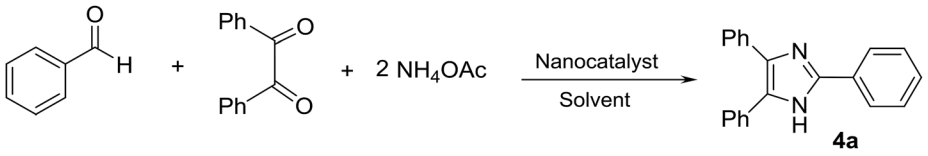

4a

Entry	Catalyst (g)	Solvent	Temperature (°C)	Time (min)	Yield[b] (%)
1	0.005	EtOH	80	90	70
2	0.010	EtOH	80	60	82
3	**0.020**	**EtOH**	**80**	**45**	**98**
4	0.030	EtOH	80	45	95
5	0.040	EtOH	80	45	93
6	0.020	MeOH	65	60	90
7	0.020	DMSO	120	60	85
8	0.020	CH_3CN	80	60	55
9	0.020	H_2O	100	90	20
10	0.020	EtOH : H_2O (1 : 1)	100	90	35
11	0.020	CH_2Cl_2	40	90	58
12	0.020	EtOH	50	90	60
13	0.020	EtOH	60	60	75
14	0.020	EtOH	70	45	92
15	Zeolite-NaY (0.02)	EtOH	80	120	15
16	SO_3H@zeolite-Y (0.02)	EtOH	80	55	90
17	—	EtOH	80	240	50

[a] Reaction conditions: benzil (1 mmol), benzaldehyde (1 mmol), ammonium acetate (2 mmol) and catalyst in solvent. [b] Isolated yield.

same reaction in the presence of 0.02 g of zeolitic catalyst was carried out at different temperatures to assess the effect of temperature on the reaction yield. The yield increased as the reaction temperature was raised. At 80 °C, the desired product was obtained in high yield within 45 min (Table 1, entry 3). A further increase in temperature and time did not improve the product yield (Table 2, entry 12). Although SO_3H@zeolite-Y showed a good catalytic effect for this reaction (Table 2, entry

Table 3 Synthesis of 2,4,5-trisubstituted imidazoles catalyzed by Fe_3O_4/SO_3H@zeolite-Y[a]

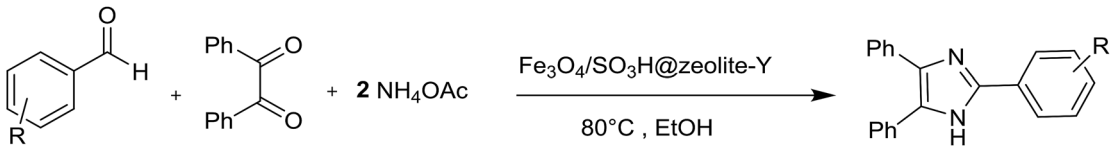

Entry	R	Product	Time (min)	Yield[b] (%)	$mp_{rep}/mp_{lit.}$ (°C)
1	H	**4a**	45	98	270–272 (271–273)[11]
2	2-NO_2	**4b**	65	97	226–228 (226–227)[37]
3	3-NO_2	**4c**	20	85	268–270 (267–268)[11]
4	3-OH, 4-OMe	**4d**	45	93	215–217 (215–217)[11]
5	2-OMe	**4e**	65	97	200–202 (209–211)[38]
6	3,4-OMe	**4f**	45	98	214–216 (214–216)[11]
7	3-OH	**4g**	35	97	259–261 (259–260)[11]
8	4-OMe	**4h**	60	95	226–228 (230–231)[11]
9	2-Cl	**4i**	65	95	168–170 (196–199)[37]
10	2,3-Cl	**4j**	50	98	254–256 (194–197)[37]
11	2,4-Cl	**4k**	50	98	168–170 (175–178)[37]
12	4-Cl	**4l**	35	97	260–262 (260–262)[11]
13	3-Br	**4m**	30	98	301–303 (302–303)[11]
14	4-Me	**4n**	45	96	231–233 (230–232)[11]

[a] Reaction conditions: benzil (1 mmol), aldehyde (1 mmol), ammonium acetate (2 mmol) and Fe_3O_4/SO_3H@zeolite-Y (0.020 g) in EtOH at 80 °C. [b] Isolated yield.

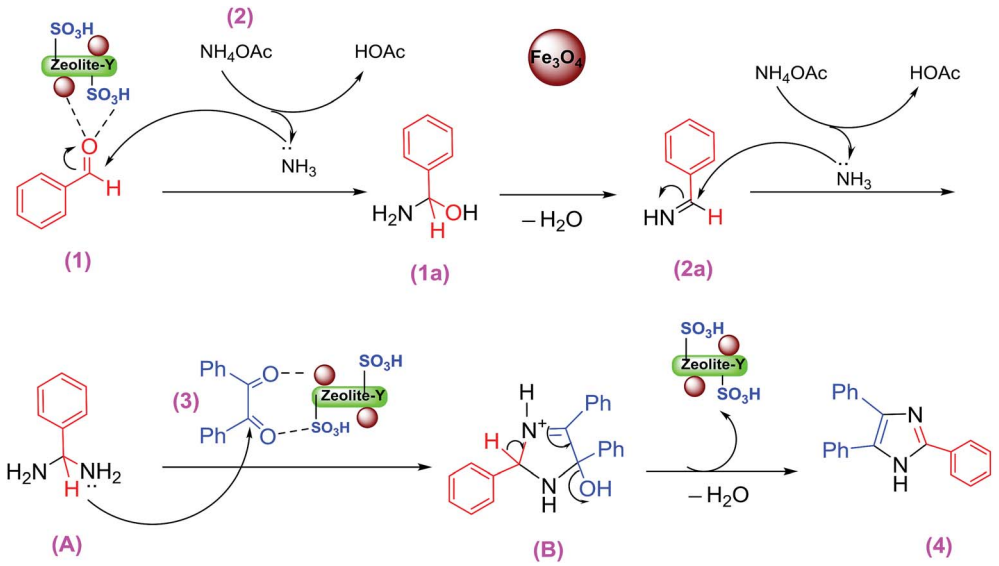

Scheme 3 The suggested mechanism of tri-substituted imidazoles synthesis.

16), but centrifugation had required in order to separate the nanocatalyst. Modern catalytic methods offer a great potential for future developments in the synthesis of heterogeneous catalysts based on magnetic nanomaterials. Magnetic separation is a simpler, faster, and cleaner way to recover the catalyst. The presence of magnetite nanoparticles also improved catalytic effect and decreased slightly at reaction time. Therefore, the Fe_3O_4/SO_3H@zeolite-Y was chosen was chosen to improve the catalytic path. Also, this condensation was performed under catalyst-free conditions. The yield of the product was 50% after 4 h (Table 2, entry 17). Therefore, the presence of the nanocatalyst was necessary for a shorter time and higher efficiency.

The scope and generality of the synthesis of 2,4,5-triaryl substituted imidazoles were studied by using various aromatic aldehydes bearing both electron-withdrawing and electron-donating groups. As the results clearly show (Table 3), this organic transformation in the presence of the zeolitic nanocomposite provided the corresponding products in high yields and appropriate reaction times (Table 3, **4a–n**).

A plausible mechanism for the formation of 2,4,5-triaryl-1*H*-imidazoles in the presence of Fe_3O_4/SO_3H@zeolite-Y catalyst is shown in Scheme 3. Fe_3O_4/SO_3H@zeolite-Y as heterogeneous multi-functional nanocatalyst facilitates this cyclocondensation due to the existence of both Lewis acid (Fe_3O_4) and Brønsted

Table 4 Optimizing the model reaction conditions for the synthesis of perimidine **6d**[a]

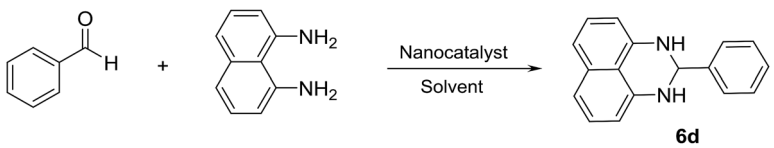

6d

Entry	Catalyst (g)	Solvent	Temperature (°C)	Time (min)	Yield[b] (%)
1	0.0047	EtOH	rt	4	81
2	**0.008**	**EtOH**	**rt**	**4**	**98**
3	0.016	EtOH	rt	4	70
4	0.008	MeOH	rt	4	80
5	0.008	DMSO	rt	4	75
6	0.008	CH_3CN	rt	10	63
7	0.008	CH_2Cl_2	rt	15	51
8	0.008	H_2O	rt	18	46
9	0.008	EtOH : H_2O (1 : 1)	rt	10	81
10	Zeolite-Y (0.008)	EtOH	rt	120	20
11	SO_3H@zeolite-Y (0.008)	EtOH	rt	8	89
12	—	EtOH	rt	120	10

[a] Reaction conditions: benaldehyde (1 mmol), 1,8-diaminonaphthalene (1 mmol), catalyst, in solvent at 25 °C. [b] Isolated yield.

Table 5 Synthesis of dihydroperimidine catalyzed by Fe_3O_4/SO_3H@zeolite-Y[a]

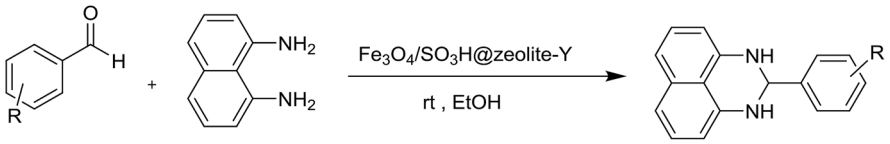

Entry	R	Product	Time (min)	Yield[b] (%)	$mp_{rep}/mp_{lit.}$ (°C)
15	H	**6a**	4	98	104–106 (104–106)[20]
16	2-NO_2	**6b**	4	98	180–192 (192–194)[20]
17	3-NO_2	**6c**	4	90	200–202(183–185)[39]
18	4-NO_2	**6d**	3	98	224–226 (201–202)[20]
19	4-OMe	**6e**	4	90	160–162 (161–163)[20]
20	3,4-OMe	**6f**	5	89	214–216 (205–207)[20]
21	2-OH	**6g**	5	90	180–182 (192–193)[40]
22	2-OH, 5-Br	**6h**	4	95	148–150 (165–166)[20]
23	2-OH, 4-OMe	**6i**	6	89	204–206 (168–169)[20]
24	3-Cl	**6j**	4	95	144–146 (145–146)[20]
25	4-Cl	**6k**	4	98	171–173 (173–174)[20]
26	2,3-Cl	**6l**	4	95	130–132 (131–133)[21b]
27	5-NO_2[c]	**6m**	6	88	340–342 (350)[20]

[a] Reaction conditions: aldehyde (1 mmol), 1,8-diaminonaphthalene (1 mmol), Fe_3O_4/SO_3H@zeolite-Y (0.008 g), in EtOH at 25 °C. [b] Isolated yield. [c] 5-Nitrofuran-2-yl.

acidic (SO_3H) sites. On the basis of the literature and substrates chemistry, the SO_3H Brønsted acid supported on Fe_3O_4 Lewis acid polarizes the carbonyl group of aldehyde. Then, hydroxylamine intermediate (**1a**) is formed by condensation reaction of an aromatic aldehyde (**1**) and NH_3 (**2**), which is then dehydrated to imine (**2a**). The addition of the second mole of NH_3 produces diamine intermediate (**A**). Condensation of diamine with benzil (**3**) followed by cyclization, dehydration, and then rearrangement through the imino intermediate (**B**) yielded the substituted imidazole product (**4**).[11]

In another synthesis procedure, the catalytic performance of Fe_3O_4/SO_3H@zeolite-Y was investigated for the synthesis of

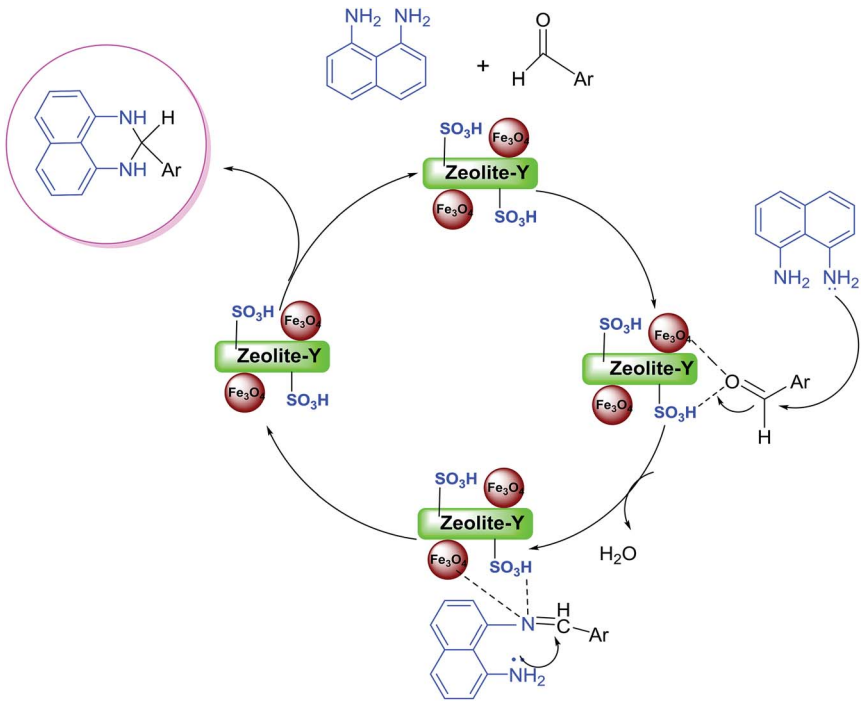

Scheme 4 The possible reaction mechanism for the synthesis of 2-aryl perimidines in the presence of Fe_3O_4/SO_3H@zeolite-Y.

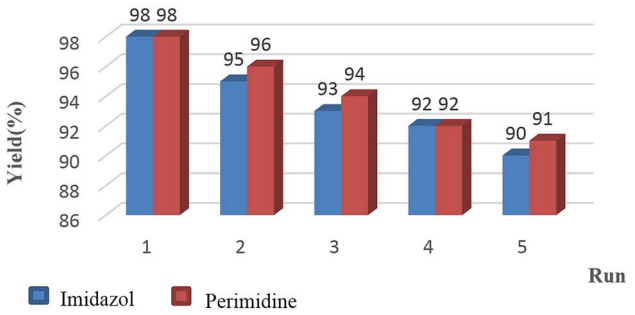

Fig. 8 Examination of Fe_3O_4/SO_3H@zeolite-Y reusability in the synthesis of imidazoles and perimidines.

dihydroperimidine derivatives (Table 4, entries 1–12). In order to optimize the reaction conditions, some parameters such as solvent, catalyst amount, and temperature, were probed for the condensation of benzaldehyde with 1,8-diaminonaphthalene as a model reaction in the presence of Fe_3O_4/SO_3H@zeolite-Y. The optimum reaction conditions were found to be use of 0.008 g of Fe_3O_4/SO_3H@zeolite-Y in the EtOH solvent at 4 min with 98% yield (Table 4, entry 2). It can be concluded that the nano-size and large surface area of the support makes the heterogenized SO_3H catalyst readily available for substrates. Further, the catalytic performance of Fe_3O_4 (as a Lewis acid) supported on the zeolite for the reaction is attributed to the large surface area of the nanocatalyst and support, which facilitate the appropriate interaction of the reactant and product molecules. Moreover, this technique makes catalyst separation from aqueous solutions more effective and simple (as a significant advantage in comparison with the SO_3H@zeolite-Y catalyst). The catalyst free reaction has no good results for the synthesis of 2-substituted 2,3-dihydro-1*H*-perimidines (Table 4, entry 12).

To extend the scope of this study, the above optimized conditions, were employed for a cyclocondensation reaction between a variety of aromatic aldehydes and 1,8-diaminonaphthalene over the Fe_3O_4/SO_3H@zeolite-Y catalyst (Table 5, **6a–m**). Based on these results, both electron-donating and electron-withdrawing groups proceed smoothly with very good efficiency to form the desired products in high yields within the very short time.

A possible mechanism (Scheme 4) is proposed for the synthesis of 2-aryl perimidines which is consistent with the literature.[21] The nucleophilic attack of diamino aromatic ring to Fe_3O_4/SO_3H@zeolite-Y-activated aldehyde generated the imine intermediate with the removal of H_2O molecule. Subsequently, nucleophilic attack of the second amino group to nanocatalyst-activated imine intermediate is followed by cyclization process to give the desired product.

The reusability and recyclability of Fe_3O_4/SO_3H@zeolite-Y catalyst was investigated in the model reactions for the preparation of tri-substituted imidazoles and 2-aryl perimidines (Fig. 8). In both of these reactions, the nanocatalyst was easily recycled at least five times without significant loss of activity. In this regard, after completion of the reaction, the catalyst was separated by an external magnet, washed with ethyl acetate and dried at 50 °C to be ready for the subsequent runs. The FTIR and

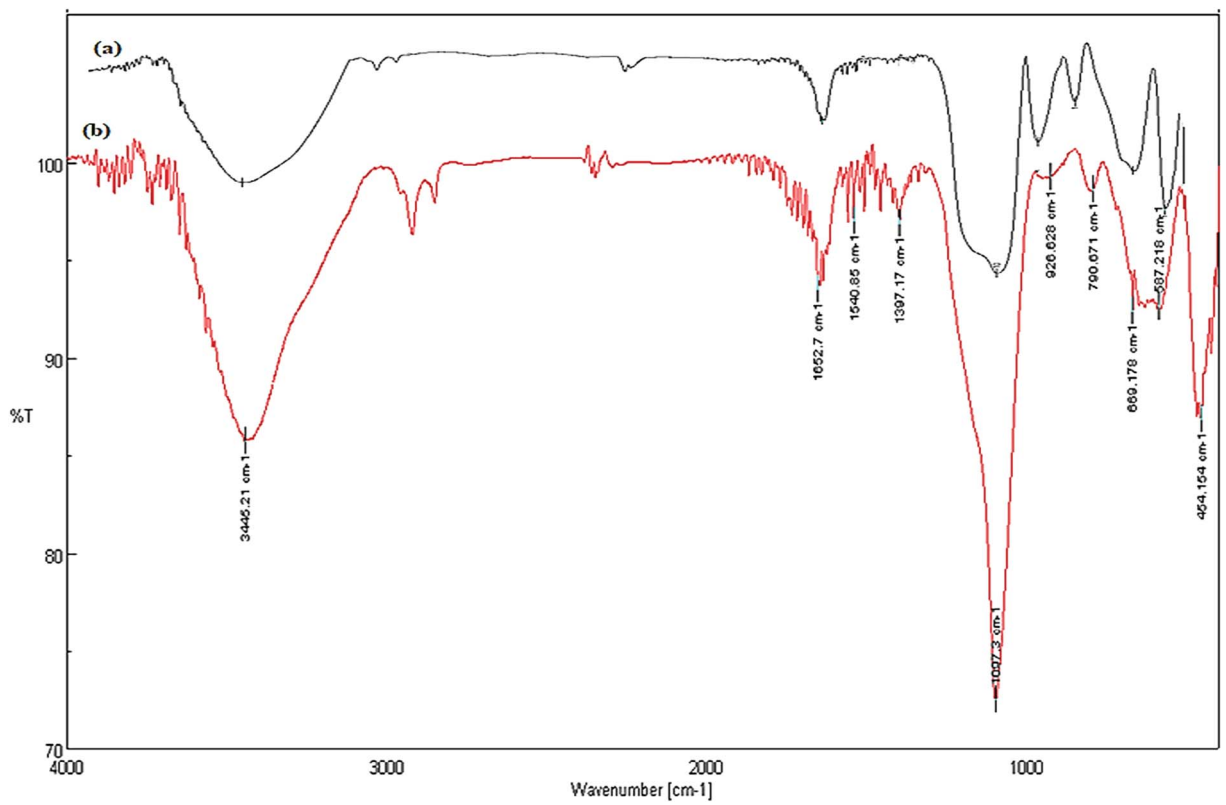

Fig. 9 FTIR spectra of (a) fresh and (b) recovered Fe_3O_4/SO_3H@zeolite-Y.

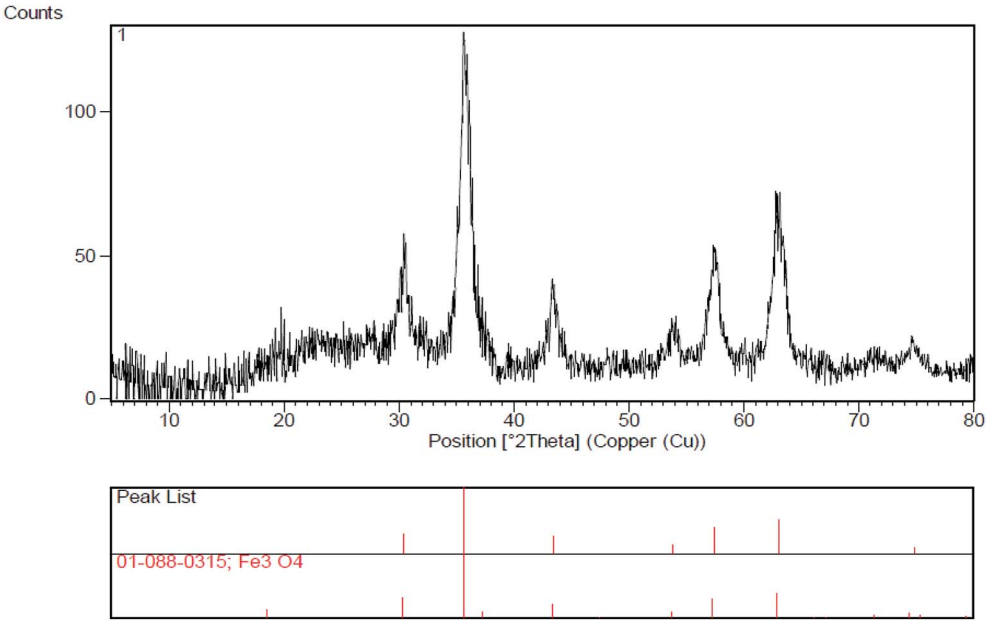

Fig. 10 XRD pattern of recovered Fe_3O_4/SO_3H@zeolite-Y.

Table 6 Comparison of the catalytic efficiency of Fe_3O_4/SO_3H@zeolite-Y with other catalysts for the synthesis of imidazoles (entries 1–8) and perimidines (entries 9–16) for their model reactions (1 mmol from the raw materials)

Entry	Catalyst/conditions	Time (h)	Yield[a] (%)
1	Fe_3O_4g-C_3N_4 (0.02 g), EtOH, 78 °C	2	95 (ref. 41)
2	Fe_3O_4@chitosan (0.05 g), EtOH, reflux	2	95 (ref. 42)
3	Benzethonium chloride (10 mole%), EtOH : H_2O, 70 °C	0.75	95 (ref. 43)
4	Sodium dodecyl-sulfate (0.02 g), H_2O, 80 °C	1	90 (ref. 44)
5	Fe_3O_4@SiO_2·HM·SO_3H (0.04 g), solvent-free, 110 °C	0.25	93 (ref. 37)
6	Fe_3O_4@SiO_2·HM·SO_3H (0.060 g), solvent-free, MWI	0.13	77 (ref. 45)
7	Sulfamic acid-Fe_3O_4 NPs (0.1 g), EtOH, reflux	2	90 (ref. 46)
8	Fe_3O_4/SO_3H@zeolite-Y (0.02 g), EtOH, 80 °C	0.75	98 (this work)
9	CuY-zeolite (0.002 g), EtOH, rt	0.42	81 (ref. 20)
10	NaY zeolite (0.2 g), EtOH, rt	45–50	70 (ref. 47)
11	$FePO_4$ (10 mol%), EtOH, rt	0.22	80 (ref. 48)
12	Ytterbium(III) trifluoromethanesulfonate (0.1 equiv.), MeCN, rt	24	88 (ref. 49)
13	$Fe_3O_4/SiO_2/(CH_2)_3N^+Me_3Br_3^-$ (0.007), solvent-free, 80 °C	12	93 (ref. 50)
14	Nano-γ-$Al_2O_3/SbCl_5$ (0.1 g), solvent-free, rt	0.25	95 (ref. 21)
15	$Cu(NO_3)_2$ (5 mole%), $2H_2O$, EtOH, rt	0.17	83 (ref. 51)
16	Fe_3O_4/SO_3H@zeolite-Y (0.008 g), EtOH, rt	0.07	98 (this work)

[a] Isolated yield.

XRD data of the recycled catalyst shows no change in its structure (Fig. 9 and 10).

Also, to show the advantages of using Fe_3O_4/SO_3H@zeolite-Y nanocatalyst in the synthesis of 2,4,5-triaryl-1*H*-imidazoles (Table 4, entries 1–8) and 2,3-dihydro-1*H*-perimidines (Table 4, entries 9–16), this catalytic method was compared with literature resulted in reports of using various catalysts for the model reactions. As shown in Table 6, in the presence of this new magnetic nanocomposite [with Lewis acid (Fe_3O_4) and Brønsted–Lowry acid (SO_3H)], the results were better than other catalysts.

3. Conclusions

In conclusion, magnetic SO_3H@zeolite-Y nanocomposite supported nano Fe_3O_4 was successfully synthesized and used for the synthesis of 2,4,5-trisubstituted imidazoles and 2-aryl perimidines under mild conditions. The most interesting features of the present method are simple preparation, the use of non-toxic nature of the nanocatalyst, easy separation of the catalyst after reaction, and substantial improvements in the reaction time and yield. The nanocatalyst was readily recycled by an external permanent magnet and could be reused five times

without any significant loss of its performance. Further applications of multi-functional nanocatalysts based on the zeolite-NaY to other green reactions are currently under investigation.

4. Experimental

4.1. Chemicals and apparatus

All chemicals were purchased from the Merck and Fluka Chemical Companies. The products were identified by comparing the physical data with those of known samples or by their spectral data. FT-IR spectra were obtained with KBr disc on a galaxy series FT-IR 5000 spectrometer. ^{1}H NMR and ^{13}C NMR spectra were recorded with a Bruker DRX-400 spectrometer at 400 and 100 MHz respectively. The surface morphology of zeolite and modified structures were analyzed by field emission scanning electron microscopy (FESEM) (EVO LS 10, Zeiss, Carl Zeiss, Germany). The magnetic measurement of samples was carried out in a vibrating sample magnetometer (VSM) (4 inch, NDKF, Kashan, Iran) at room temperature. Diffuse reflectance spectra were acquired on an X-ray photoelectron spectrometer (Escalab 250Xi). Nitrogen adsorption and desorption isotherms (BET analysis) were measured at 196 °C by a Japan Belsorb II system after the samples were vacuum dried at 150 °C overnight.

4.2. Synthesis of Fe_3O_4/SO_3H@zeolite-Y

For preparation of SO_3H@zeolite-Y, a 500 mL flask was equipped with a constant pressure dropping funnel containing 3 mL of $ClSO_3H$. Then, 1.5 g of zeolite-NaY was charged into the flask and $ClSO_3H$ was added dropwise manner to zeolite-NaY over a period of 30 min. at 0 °C. After the addition was complete, the mixture was stirred for 45 min. Afterwards, the mixture was washed with CH_2Cl_2 and H_2O under sonication and dried at 50 °C. In continue, nano magnetic zeolosulforic acid (NMSZ) was prepared by a chemical co-precipitation process as described by Mesdaghinia *et al.*[34] $FeCl_2 \cdot 4H_2O$ (2.3 mmol, 0.45 g) and $FeCl_3 \cdot 6H_2O$ (4.6 mmol, 1.23 g) precursors (1 : 2, molar ratio) were dissolved in 25 mL of water and 1 g of SO_3H@zeolite-Y were dispersed in this aqueous solution under N_2 atmosphere bubbling for 1 h. Then, 20 mL of ammonium hydroxide (25%) was added to the mixture. The mixture was stirred at 90 °C for 30 minutes. The black precipitate was extracted by an external magnet and washed with HCl solution (0.1 M), double-distilled water and dried at 70 °C in vacuum oven to obtain the Fe_3O_4/SO_3H@zeolite-Y nanocomposite.

4.3. General procedure for the synthesis of 2,4,5-triaryl substituted imidazoles

A mixture of benzil (1 mmol, 0.210 g), aldehyde (1 mmol), ammonium acetate (2 mmol, 0.154 g) and Fe_3O_4/SO_3H@zeolite-Y (0.020 g) in EtOH was stirred at 80 °C. After completion of the reaction (TLC monitoring using *n*-hexane and ethyl acetate, 9 : 1), the nanocatalyst was separated by magnetic decantation and the solvent was evaporated. The crude product was either recrystallized from aqueous-acetone and air dried. The products were characterized by comparing the results of physical and spectroscopic data with those of the authentic samples. Characterization data for some of the imidazole compounds are given below.

2-(3-Nitrophenyl)-4,5-diphenyl-1*H*-imidazole (4c). FTIR (KBr) ν (cm^{-1}): 3434 (N–H), 1627 (C=C), 1524 (C=N), 14.89 (N=O), 1348 (N–O); ^{1}H NMR (DMSO-d_6, 400 MHz) δ (ppm): 7.14–7.16 (m, 5H, Ar–H), 7.38–7.44 (m, 5H, Ar–H), 7.47 (d, 1H, ^3J = 7.6 Hz, Ar–H), 8.00 (d, 1H, ^3J = 7.6 Hz, Ar–H), 8.46 (d, 1H, ^3J = 7.6 Hz, Ar–H), 8.48 (d, 1H, ^3J = 7.6 Hz, Ar–H), 8.91 (s, 1H, Ar–H), 9.8 (s, 1H, N–H).

2-(3-Hydroxy, 4-methoxyphenyl)-4,5-diphenyl-1*H*-imidazole (4d). FTIR (KBr) ν (cm^{-1}): 3530 (N–H), 1594 (C=C), 1499 (C=N); ^{1}H NMR (DMSO-d_6, 400 MHz) δ (ppm): 2.77 (s, 3H, CH_3), 6.75 (d, 1H, ^3J = 8.4 Hz, Ar–H), 7.14–716 (m, 6H, Ar–H), 7.35–7.39 (m, 5H, Ar–H), 7.49 (s, 1H, Ar–H), 7.53 (s, 1H, OH), 7.8 (s, 1H, N–H).

2-(3-Hydroxyphenyl)-4,5-diphenyl-1*H*-imidazole (4g). FTIR (KBr) ν (cm^{-1}): 3373 (N–H), 1590 (C=C), 1479 (C=N); ^{1}H NMR (DMSO-d_6, 400 MHz) δ (ppm): 6.98 (t, 2H, ^3J = 8 Hz, Ar–H), 7.06–7.10 (m, 4H, Ar–H), 7.11–7.16 (m, 5H, Ar–H), 7.41–7.43 (m, 4H, Ar–H), 7.46 (s, 1H, OH), 8.8 (s, 1H, N–H).

2-(3-Bromophenyl)-4,5-diphenyl-1*H*-imidazole (4m). FTIR (KBr) ν (cm^{-1}): 3432 (N–H), 1599 (C=C), 1455 (C=N); ^{1}H NMR (DMSO-d_6, 400 MHz) δ (ppm): 7.34–7.35 (m, 7H, Ar–H), 7.51–7.56 (m, 5H, Ar–H), 7.89 (s, 1H, Ar–H), 8.13 (s, 1H, Ar–H), 9.9 (s, 1H, N–H).

2-(4-Methylphenyl)-4,5-diphenyl-1*H*-imidazole (4n). FTIR (KBr) ν (cm^{-1}): 3431 (N–H), 1601 (C=C), 1497 (C=N); ^{1}H NMR (DMSO-d_6, 400 MHz) δ (ppm): 2.30 (s, 3H, CH_3), 7.14–7.20 (d, 3H, ^3J = 7.2 Hz, Ar–H), 7.21–7.30 (m, 5H, Ar–H), 7.49–7.50 (m, 4H, Ar–H), 7.92 (d, 2H, ^3J = 7.2 Hz, Ar–H), 10.0 (s, 1H, N–H).

4.4. General procedure for the preparation of 2-substituted 2,3-dihydro-1*H*-perimidines

A mixture of aldehyde (1 mmol), 1,8-diaminonaphthalene (1 mmol, 0.158 g), Fe_3O_4/SO_3H@zeolite-Y (0.008 g), in EtOH was stirred at 25 °C. After completion of the reaction, (TLC monitoring using hexane and ethyl acetate, 3 : 1), the nanocatalyst was separated by magnetic field. A mixture of ice and water was added to the filtrate and the precipitate product was obtained by filtration and washed thoroughly with water–ethanol mixture. The product was purified by recrystallization in ethanol–water and identified by physical and spectroscopic techniques. Characterization data for some of the compounds are given below.

2-(2-Nitrophenyl)-2,3-dihydro-1*H*-perimidine (6b). FT-IR (KBr, ν_{max}): 3357, 3230 (N–H), 2921 (C–H), 1518, 1333 (NO_2), 1601, 1414, 1347 (C=C), 1165, 1125, 1031 (C–N), 826, 758 cm^{-1}; ^{1}H NMR (300 MHz, DMSO-d_6): δ_H 8.03 (d, J = 8.11 Hz, 1H, H–Ar), 7.88 (d, J = 7.92 Hz, 1H, H–Ar), 7.75–7.64 (m, 2H, H–Ar), 7.18 (t, J = 8.10 Hz, 2H, H–Ar), 7.03 (d, J = 8.25 Hz, 2H, H–Ar), 6.82 (br, 2H, NH), 6.53 (d, J = 7.5 Hz, 2H, H–Ar), 5.82 (s, 1H, N–CH–N) ppm; ^{13}C NMR (75 MHz, DMSO-d_6): δ = 149.3, 142.5, 136.9, 134.6, 134.0, 130.4, 130.0, 127.5, 124.4, 116.2, 112.5, 105.2, 61.4 ppm.

2-(2-Hydroxy-4-methoxyphenyl)-2,3-dihydro-1*H*-perimidine (6i). FT-IR (KBr, ν_{max}): 3420 (NH, OH), 2916 (C–H), 1600, 1420

(C=C), 1257, 1107 (C–O), 1028 (C–N), 811, 759, 418 cm^{-1}; ^1H NMR (300 MHz, DMSO-d_6): δ_H 9.70 (s, 1H, OH), 7.35 (d, J = 8.82 Hz, 1H, H–Ar), 7.22–7.11 (m, 2H, H–Ar), 6.96 (d, J = 8.05 Hz, 2H, H–Ar), 6.52–6.43 (m, 6H, H–Ar and NH), 5.57 (s, 1H, N–CH–N), 3.70 (s, 3H, OCH_3) ppm; ^{13}C NMR (75 MHz, DMSO-d_6): δ_C 160.6, 156.9 (C–O), 143.9, 134.8, 129.8, 127.2, 127.2, 120.0, 115.7, 112.9, 104.9, 101.5, 61.1 (N–C–N), 55.4 (OCH_3) ppm.

2-(2,3-Dichlorophenyl)-2,3-dihydro-1*H*-perimidine (6l). FT-IR (KBr) (ν_{max}): 3348, 3235 (N–H), 3044 (C–H), 1625, 1600, 1493, 1420, 1403, 1382, 1265 (C=C), 1182, 1161, 1043 (C–N), 835, 787, 757 (C–Cl), 603 cm^{-1}; ^1H NMR (500 MHz, DMSO-d_6): δ_H 7.69 (d, J = 8.15 Hz, 2H, H–Ar), 7.45 (t, J = 7.90 Hz, 1H, H–Ar), 7.19 (t, J = 7.78 Hz, 2H, H–Ar), 7.04 (d, J = 8.15 Hz, 2H, H–Ar), 6.83 (s, 2H, NH), 6.52 (d, J = 7.35 Hz, 2H, H–Ar), 7.83 (s, 1H, N–CH–N) ppm; ^{13}C NMR (125 MHz, DMSO-d_6): δ_C 142.7, 141.8, 134.7, 132.1, 131.1, 130.7, 128.8, 128.6, 127.3, 116.1, 112.5, 105.0, 63.5 (N–CH–N) ppm.

2-(5-Nitrofuran-2-yl)-2,3-dihydro-1*H*-perimidine (6m). FT-IR (KBr, ν_{max}): 3434 (N–H), 1603, 1480 (C=C), 1520, 1360 (–NO_2), 1020 (C–N), 808, 601 cm^{-1}; ^1H NMR (300 MHz, DMSO-d_6): δ_H 8.25 (d, J = 7.00 Hz, 2H, H–Ar), 7.69 (s, 2H, H–Ar), 7.52–7.27 (m, 6H, H–Ar and 2NH), 5.25 (s, 1H, N–CH–N) ppm; ^{13}C NMR (75 MHz, DMSO-d_6): δ_C 161.3, 150.2, 137.0, 135.5, 130.1, 128.4, 124.4, 119.2, 116.1, 114.6, 69.7 (N–C–N) ppm.

Conflicts of interest

There are no conflicts to declare.

Acknowledgements

We are thankful to the Payame Noor University for the partial support of this work.

References

1 L. Zhang, X. M. Peng, G. L. Damu, R. X. Geng and S. H. Zhou, *Med. Res. Rev.*, 2014, **34**, 340–437.

2 (*a*) M. Zendehdel, A. Mobinikhaledi, H. Alikhani and N. Jafari, *J. Chin. Chem. Soc.*, 2010, **57**, 683–689; (*b*) A. Mobinikhaledi, M. A. Bodaghi Fard, F. Sasani and M. A. Amrollahi, *Bulg. Chem. Commun.*, 2013, **45**, 353–356.

3 Y. L. Fan, X. H. Jin, Z. P. Huang, H. F. Yu, Z. G. Zeng, T. Gao and L. S. Feng, *Eur. J. Med. Chem.*, 201, **15**, 347–365.

4 (*a*) K. Undheim and C. Benneche, in *Comprehensive Heterocyclic Chemistry II*, ed. A. R. Katritzky, C.W. Rees and E. F. Scriven, Pergamon, Oxford, 1996; (*b*) A. F. Pozharskii and V. V. Dalnikovskaya, *Russ. Chem. Rev.*, 1981, **50**, 816–835; (*c*) X. Bu, L. W. Deady, G. J. Finlay, B. C. Baguley and W. A. Denny, *J. Med. Chem.*, 2001, **44**, 2004–2014; (*d*) J. M. Herbert, P. D. Woodgate and W. A. Denny, *J. Med. Chem.*, 1987, **30**, 2081–2086; (*e*) D. R. Luthin, A. K. Rabinovich, D. R. Bhumralkar, K. L. Youngblood, R. A. Bychowski, D. S. Dhanoa and J. M. May, *Bioorg. Med. Chem. Lett.*, 1999, **9**, 765–770; (*f*) F. A. Bassyouni, S. M. Abu-Bakr, K. H. Hegab, W. El-Eraky, A. A. El Beih and M. E. Abdel Rehim, *Res. Chem. Intermed.*, 2012, **38**, 1527–1528.

5 (*a*) J. G. Lambardino and E. H. Wiseman, *J. Med. Chem.*, 1974, **17**, 1182–1188; (*b*) A. Puratchikody and M. Doble, *Bioorg. Med. Chem. Lett.*, 2007, **15**, 1083–1090; (*c*) J. G. Lombardino and E. H. Wiseman, *J. Med. Chem.*, 1974, **17**, 1182–1188; (*d*) J. G. Lombardino, *US Pat.*, 3772441, 1973; (*e*) T. Maier, R. Schmierer, K. Bauer, H. Bieringer, H. Buerstell and B. Sachse, *US Pat.*, 4820335, 1989; (*f*) U. Ucucu, I. Iskdag and B. Cakir, *Gazi Univ. Eczacilik Fak. Derg.*, 1988, **5**, 161–165; (*g*) S. E. Wolkenberg, D. D. Wisnoski, W. H. Leister, Y. Wang, Z. Zhao and C. W. Lindsley, *Org. Lett.*, 2004, **6**, 1453–1456.

6 K. V. Belyaeva, L. V. Andriyankova, L. P. Nikitina, A. G. Mal'kina, A. V. Afonin and B. A. Trofimov, *Tetrahedron Lett.*, 2012, **53**, 7040–7043.

7 (*a*) T. A. Farghaly, M. A. Abdallah and Z. A. Muhammad, *Res. Chem. Intermed.*, 2015, **41**, 3937–3947; (*b*) F. A. Bassyouni, S. M. Abu-Bakr, K. H. Hegab, W. El-Eraky, A. A. E. Beih and M. E. A. Rehim, *Res. Chem. Intermed.*, 2012, **38**, 1527–1550.

8 J. L. Davis, M. G. Papich and M. C. Heit, Antifungal and Antiviral Drugs, in *Veterinary Pharmacology and Therapeutics*, ed. J. E. Riviere and M. G. Papich, Wiley-Blackwell, 9th edn, 2009, ch. 39, vol. 1019–1020, ISBN 978-0-8138-2061-3.

9 (*a*) N. Xi, Q. Huang and L. Liu, in *comprehensive heterocyclic chemistry III*, ed. A. R. Katritzky, C. A. Ramsden, E. F. V. Scriven and R. J. K. Taylor, Elsevier science, Oxford, 2008, vol 4, pp. 143–348; (*b*) L. De Luca, *Curr. Med. Chem.*, 2006, **13**, 1–23.

10 H. Debus, *Ann. Chem. Pharm.*, 1858, **107**, 199–208.

11 Z. Zarnegar and J. Safari, *New J. Chem.*, 2014, **38**, 4555–4565.

12 K. F. Shelke, S. B. Sapkal, S. S. Sonar, B. R. Madje, B. B. Shingate and M. S. Shingare, *Bull. Korean Chem. Soc.*, 2009, **30**, 1057–1060.

13 S. D. Jadhave, N. D. Kokare and S. D. Jadhave, *J. Heterocycl. Chem.*, 2009, **45**, 1461–1464.

14 A. Shaabani, A. Rahmati, E. Farhangi and Z. Badri, *Catal. Commun.*, 2007, **8**, 1149–1152.

15 H. Weinmann, M. Harre, K. Koeing, E. Merten and U. Tilestam, *Tetrahedron Lett.*, 2002, **43**, 593–595.

16 J. Liu, J. Chen, J. Zhao, Y. Zhao, L. Li and H. Zhang, *Synthesis*, 2003, 2661–2666.

17 M. M. Khodaei, K. Bahrami and I. Kavianinia, *J. Chin. Chem. Soc.*, 2007, **54**, 829–833.

18 N. D. Kokare, J. N. Sangshetti and D. B. Shinde, *Synthesis*, 2007, 2829–2834.

19 (*a*) V. Paragamian, M. B. Baker, B. M. Puma and J. Reale, *J. Heterocycl. Chem.*, 1968, **5**, 591–597; (*b*) A. Shaabani and A. Maleki, *Chem. Pharm. Bull.*, 2008, **56**, 79–81; (*c*) J. B. Hendrickson and M. S. Hussoin, *J. Org. Chem.*, 1987, **52**, 4137–4139; (*d*) J. J. Vanden Eynde, F. Delfosse, A. Mayence and Y. V. Haverbeke, *Tetrahedron*, 1995, **51**, 5813–5818; (*e*) I. Yavari, H. Mostafavi, D. Tahmassebi and R. Hekmat-Shoar, *Monatsh. Chem.*, 1997, **128**, 675–679; (*f*) V. A. Ozeryanskii, E. A. Filatova, V. I. Sorokin and A. F. Pozharskii, *Russ. Chem. Bull.*, 2001, **50**, 846–853.

20 M. Kalhor and N. Khodaparast, *Res. Chem. Intermed.*, 2015, **41**, 3235–3242.
21 (*a*) A. Bamoniri, B. B. F. Mirjalili and S. Saleh, *RSC Adv.*, 2018, **8**, 6178–6182; (*b*) M. Kalhor, F. Rezaee-Baroonaghi, A. Dadras and Z. Zarnegar, *Appl. Organomet. Chem.*, 2019, e4784.
22 E. Doustkhah and S. Rostamnia, *J. Colloid Interface Sci.*, 2016, **478**, 280–287.
23 H. Kefayati, M. Golshekan, S. Shariati and M. Bagheri, *Chin. J. Catal.*, 2015, **36**, 572–578.
24 F. Bonyasi, M. Hekmati and H. Veisi, *J. Colloid Interface Sci.*, 2017, **496**, 177–187.
25 J. Safari and Z. Zarnegar, *J. Mol. Catal. A: Chem.*, 2013, **379**, 269–276.
26 X. N. Zhao, G. F. Hu, M. Tang, T. T. Shi, X. L. Guo, T. T. Li and Z. H. Zhang, *RSC Adv.*, 2014, **4**, 51089–51097.
27 E. Tabrizian and A. Amoozadeh, *RSC Adv.*, 2016, **6**, 96606–96615.
28 C. Zhang, H. Wang, F. Liu, L. Wang and H. He, *Cellulose*, 2013, **20**, 127–134.
29 G. Perot and M. Guisnet, *J. Mol. Catal.*, 1990, **61**, 173–196.
30 M. Kalhor, S. Banibairami and S. A. Mirshokraie, *Green Chem. Lett. Rev.*, 2018, **11**, 334–344.
31 R. Estevez, I. Iglesias, D. Luna and F. M. Bautista, *Molecules*, 2017, **22**, 2206–2217.
32 N. Krathumkhet, K. Vongjitpimol, T. Chuesutham, S. Changkhamchom, K. Phasuksom, A. Sirivata and K. Wattanakul, *Solid State Ionics*, 2018, **319**, 278–284.
33 H. Nur, G. L. Kee, H. Hamdan, T. M. I. Mahlia, J. Efendi and H. S. C. Metselaar, *Int. J. Hydrogen Energy*, 2012, **37**, 12513–12521.
34 A. Mesdaghinia, A. Azari, R. N. Nodehi, K. Yaghmaeian, A. K. Bharti, S. Agarwal, V. K. Gupta and K. Sharafi, *J. Mol. Liq.*, 2017, **233**, 378–390.
35 F. Rouquerol, J. Rouquerol and K. S. W. Sing, *Adsorption by powders and porous solids*, Academic Press, 1999, pp. 1–25.
36 M. M. Khakzad Siuki, M. Bakavoli and H. Eshghi, *Appl. Organomet. Chem.*, 2018, **32**, e4290.
37 H. Naeimi and D. Aghaseyedkarimi, *Dalton Trans.*, 2016, **45**, 1243–1253.
38 K. Nikoofar, M. Haghighi, M. Lashanizadegan and Z. Ahmadvand, *J. Taibah Univ. Sci.*, 2015, **9**, 570–578.
39 M. A. Bodaghifard, S. Asadbegi and Z. Bahrami, *J. Iran. Chem. Soc.*, 2017, **14**, 365–376.
40 O. Maloshitskaya, J. Sinkkonen, V. V. Ovcharenko, K. N. Zelenin and K. Pihlaja, *Tetrahedron*, 2004, **60**, 6913–6921.
41 T. S. Ahooie, N. Azizi, I. Yavari and M. M. Hashemi, *J. Iran. Chem. Soc.*, 2018, **15**, 855–862.
42 Z. Zarnegar and J. Safari, *RSC Adv.*, 2014, **4**, 20932–20939.
43 D. Parthiban and R. J. Karunakaran, *Orient. J. Chem.*, 2018, **34**, 3004–3015.
44 R. Bansal, P. K. Soni and A. K. Halve, *J. Heterocycl. Chem.*, 2018, **55**, 1308–1312.
45 H. Naeimi and D. Aghaseyedkarimi, *New J. Chem.*, 2015, **39**, 9415–9421.
46 J. Safari and Z. Zarnegar, *Ultrason. Sonochem.*, 2013, **20**, 740–746.
47 A. Mobinikhaledi and N. Foroughifar, *Turk. J. Chem.*, 2009, **33**, 555–560.
48 F. K. Behbahani and F. M. Golchin, *J. Taibah Univ. Sci.*, 2017, **11**, 85–89.
49 C. K. Wu, T. J. Liou, H. Y. Wei, P. S. Tsai and D. Y. Yang, *Tetrahedron*, 2014, **70**, 8219–8225.
50 A. Farrokhi, K. Ghodrati and I. Yavari, *Catal. Commun.*, 2015, **63**, 41–46.
51 A. Mobinikhaledi and P. Steel, *Synth. React. Inorg., Met.-Org., Nano-Met. Chem.*, 2009, **39**, 133–135.